Current Biology, Vol. 14, 942–952, June 8, 2004, ©2004 Elsevier Ltd. All rights reserved. DOI 10.1016/j.cub.2004.05.046

Dynamics of Centromere and Kinetochore Proteins: Implications for Checkpoint Signaling and Silencing

Jagesh V. Shah,[1] Elliot Botvinick,[2,3] Zahid Bonday,[1] Frank Furnari,[1] Michael Berns,[2,3] and Don W. Cleveland[1]
[1]Ludwig Institute for Cancer Research
Department of Cellular and Molecular Medicine and
[2]Department of Bioengineering
University of California at San Diego
La Jolla, California 92093
[3]Beckman Laser Institute
Department of Biomedical Engineering
University of California at Irvine
Irvine, California 92597

Summary

Background: The mitotic checkpoint prevents the onset of anaphase before all chromosomes are attached to spindle microtubules. The checkpoint is thought to act by the catalytic generation at unattached kinetochores of a diffusible "wait signal" that prevents anaphase. Mad2 and Cdc20, two candidate proteins for components of a diffusible wait signal, have previously been shown to be recruited to and rapidly released from unattached kinetochores.
Results: Fluorescence recovery after photobleaching demonstrated that Mad1, Bub1, and a portion of Mad2, all essential mitotic-checkpoint components, are stably bound elements of unattached kinetochores (as are structural centromere components such as Centromere protein C [CENP-C]). After microtubule attachment, Mad1 and Mad2 are released from kinetochores and relocalize to spindle poles, whereas Bub1 remains at kinetochores.
Conclusions: A long residence time at kinetochores identifies Bub1, Mad1, and a portion of Mad2 as part of a catalytic platform that recruits, activates, and releases a diffusible wait signal that is partly composed of the rapidly exchanging portion of Mad2. The release of Mad1 and Mad2, but not Bub1, from kinetochores upon attachment separates the elements of this "catalytic platform" and thereby silences generation of the anaphase inhibitor despite continued rapid cycling of Mad2 at spindle poles.

Introduction

Genomic integrity is maintained by a number of checkpoints that act during each cell cycle. The prevention of gross chromosome missegregation and the resulting aneuploidy is carried out by the mitotic checkpoint (also referred to as the spindle assembly checkpoint; for review, see [1, 2]). This signaling network precludes the onset of anaphase until each chromosome has successfully attached, through its kinetochore, to spindle microtubules. Unattached kinetochores are thought to generate and release an inhibitor that prevents an E3 ubiquitin ligase, the anaphase-promoting complex or cyclosome (APC/C), from ubiquitinating substrates (e.g., securin) whose proteosome-mediated destruction is required for advance to anaphase [3, 4]. The APC/C's activity is regulated by a variety of factors during the cell cycle (for review, see [5]). During activation of the mitotic checkpoint, Cdc20 is responsible for directing the APC/C toward targets that promote the onset of anaphase. The mitotic checkpoint is thought to act by preventing the association of Cdc20 with the APC/C or by preventing Cdc20 bound to APC/C from productively recognizing the substrates whose ubiquitination (and subsequent destruction) is required for anaphase. Thus, each unattached kinetochore is thought to generate a "wait-anaphase" signal that acts upon Cdc20 to prevent anaphase.

The current body of evidence indicates that a single unattached kinetochore is sufficient to prevent the onset of anaphase [6, 7] through the production of one or more wait-anaphase signals. Signal generation requires action of at least three kinetochore bound kinases (Mps1, Bub1 [Budding uninhibited by benzimidazole 1], and BubR1), implicating the catalytic production of such a wait signal. For example, activation of BubR1 kinase activity at kinetochores, via binding to the kinetochore-associated microtubule binding kinesin CENP-E [8, 9], is essential for a single unattached kinetochore to produce a checkpoint signal that is sufficiently robust to block progression to anaphase. Further evidence consistent with a catalytic cycle was provided by fluorescence recovery after photobleaching (FRAP) experiments in which an essential [10] mitotic-checkpoint component, Mad2 (Mitotic arrest-deficient 2), was shown to rapidly release and rebind at unattached kinetochores with a half recovery time of approximately 25 s [11]. Because Mad2 can bind Cdc20 directly and inhibit APC/C activity, the turnover at unattached kinetochores has been posited to represent the generation (and release) of a Mad2-containing wait-anaphase signal [4, 12, 13]. Cdc20 itself has also been shown to turn over at kinetochores with an even faster half recovery time of approximately 5 s [14], although this turnover is independent of microtubule attachment.

A missing component of this model, however, is a set of proteins responsible for the recruitment, production, and release of a wait signal, i.e., the factors that facilitate the proposed catalysis. One important characteristic of components of such a catalytic kinetochore scaffold would be a long residence time at unattached kinetochores and therefore a long recovery time after photobleaching. In addition, this catalytic machinery would be expected to be deactivated by microtubule attachment or subsequent tension developed thereafter. The chicken homologs of Nuf2 and Hec1/Ndc80 have recently been shown to be stably bound to unattached kinetochores [15]. However, these proteins most likely play a role in kinetochore integrity [16, 17] rather than in the direct production of the wait signal. To date, proteins

Correspondence: dcleveland@ucsd.edu

directly implicated in checkpoint signaling (e.g., Mad2 and Cdc20) have been shown to be transient elements of the unattached kinetochore, with each rapidly releasing and rebinding within a few seconds. This has led to a prediction [17, 18] that other components, particularly the Mad2 binding partner Mad1, may be stably associated after initial kinetochore binding and serve to recruit Mad2 and Cdc20 to unattached kinetochores and facilitate their rapid conversion into a form(s) that inhibits Cdc20's ability to activate APC/C for ubiquitination of mitotic substrates. We now test a central aspect of this model for checkpoint signal generation; using FRAP, we demonstrate that Mad1, Bub1, and Mad2 are, in part, stably associated with unattached kinetochores and form a combined catalytic/recruiting element of a kinetochore scaffold for generation of a wait-anaphase signal.

Results

Stable Expression of Human Mad1 Fused to Enhanced Yellow Fluorescent Protein Recapitulates Endogenous Mad1 Localization

To visualize and measure the dynamics of Mad1 during the cell cycle, we generated polyclonal lines of PTK2 (Potoroo kidney epithelium) cells to stably express enhanced yellow fluorescent protein (EYFP or YFP) fusions with human Mad1 (HsMad1). Qualitative analysis of the stable lines indicated an approximately 10% variation in expression between individual cells, most likely because of selection by FACS. In contrast with aberrant nuclear morphology described previously after transient expression of high levels of human Mad1 [20], there were no overt defects in cell or nuclear morphology, and cells proceeded through mitosis like the parental cells. Quantitative immunoblotting with an antibody raised against human Mad1 yielded maximal estimates (Figure 1A) of the levels of the HsMad1 fusions to be approximately 1.5-fold and 5-fold (for C-terminal and N-terminal fusions, respectively) that of the endogenous Mad1 level. However, because the antibody affinity for the PTK2 Mad1 (PtMad1) homolog is very likely to be significantly lower than for hsMad1, the actual levels were almost certainly significantly lower than these estimates, which is consistent with the absence of an effect on nuclear morphology or mitosis.

When antibodies against nuclear pore complex proteins, centromere proteins, and γ-tubulin were used, the Mad1 fusion proteins localized as expected for endogenous Mad1 [20]. Both Mad1 fusions were enriched at the nuclear envelope in interphase (Figure 1B), at unattached kinetochores in prophase and prometaphase (Figure 1C), and at spindle poles from prometaphase until late telophase (Figures 1D and 1E). Live-cell images confirmed that Mad1 was concentrated in a punctate pattern at the nuclear envelope (Figure 1F, small cyan arrowheads), consistent with a nuclear pore distribution, and during mitosis revealed a significant soluble pool that was difficult to appreciate in fixed-cell preparations. As cells entered mitosis, Mad1/YFP fusions accumulated at unattached kinetochores, as seen from the distinct double dot pattern (Figure 1F, red arrows). After complete nuclear-envelope disassembly, additional Mad1 bound to unattached kinetochores (Figure 1F, red arrows). Kinetochore-associated Mad1 diminished as microtubules attached; almost all (36 of 37) cells proceeded to anaphase after all kinetochores had lost detectable Mad1 (Figure 1F). After microtubule attachment and during chromosome congression, Mad1 redistributed to spindle poles (Figures 1F and 1G, large green arrowheads) and along kinetochore fibers (Figure 1G, double yellow arrowheads). Mad1 was detectable at spindle poles throughout anaphase and the onset of cytokinesis (Figures 1G, large green arrowheads), decreased at the poles by late telophase, and reassembled at the nuclear envelope in the subsequent interphase (Figure 1H, small blue arrowheads).

Mad1 Is a Stable Component of Unattached Kinetochores, Spindle Poles, and the Nuclear Envelope

The dynamics of Mad1 release and rebinding were followed by FRAP with cells expressing the YFP-tagged Mad1 fusions. Most Mad1 at unattached kinetochores did not exchange with the soluble cytoplasmic pool (percent of initial fluorescence recoverd (R%) = 24.4% $\pm$ 4.9 standard error of the mean [SEM], n = 18) (Figures 2B and 2E), even when the mitotic checkpoint signaling was maximal after nocodazole-induced microtubule disassembly (R% = 12.5% $\pm$ 1.9 SEM, n = 29, Figure 2E). The portion (approximately 10%–20%) that did release and recover did so very rapidly, with a half-recovery time of approximately 6 s during normal mitosis ($t_{1/2}$ = 5.5 s $\pm$ 1.3 SEM) or approximately 14 s in nocodazole-blocked cells ($t_{1/2}$ = 13.5 s $\pm$ 2.0 SEM) (Figure 2E).

Redistribution of Mad1 to spindle poles late in mitosis revealed that, as for Mad1 at unattached kinetochores, most (approximately 80%) was stably bound (R% = 21.9% $\pm$ 2.7 SEM, n = 39) (Figures 2B and 2F). The small cycling pool showed rapid kinetics ($t_{1/2}$ = 6.6 s $\pm$ 1.1 SEM) that were not significantly different from recovery times measured at kinetochores in normal mitoses or in nocodazole-blocked mitotic cells (Figure 2F). After nuclear reassembly in early G1 and throughout interphase, Mad1 was stably bound at the nuclear envelope (Figures 2A and 2D). Neither N- nor C-terminal YFP fusions recovered significantly within 15 min after photobleaching (R% $<$ 20%, $t_{1/2} >$ 15 min, n = 21 cells, Figures 2A and 2D) at the nuclear envelope or within the nucleoplasm.

Mitosis-Specific Rapid Exchange of Mad2 Bound to Immobilized Mad1

In contrast to the stability of Mad1 binding to kinetochores prior to microtubule capture, Mad2 has previously been demonstrated to cycle rapidly at such kinetochores [11]. To test if this dynamic release and rebinding was selective during mitosis, we generated polyclonal PTK2 lines expressing human Mad2 fused to YFP (hsMad2/YFP). Qualitative analysis of polyclonal lines indicated that there was an approximately 20% variation between individual cells. There were no gross changes in mitotic progression (n = 51 cells); however, stable expression of YFP fusions did result in a slight

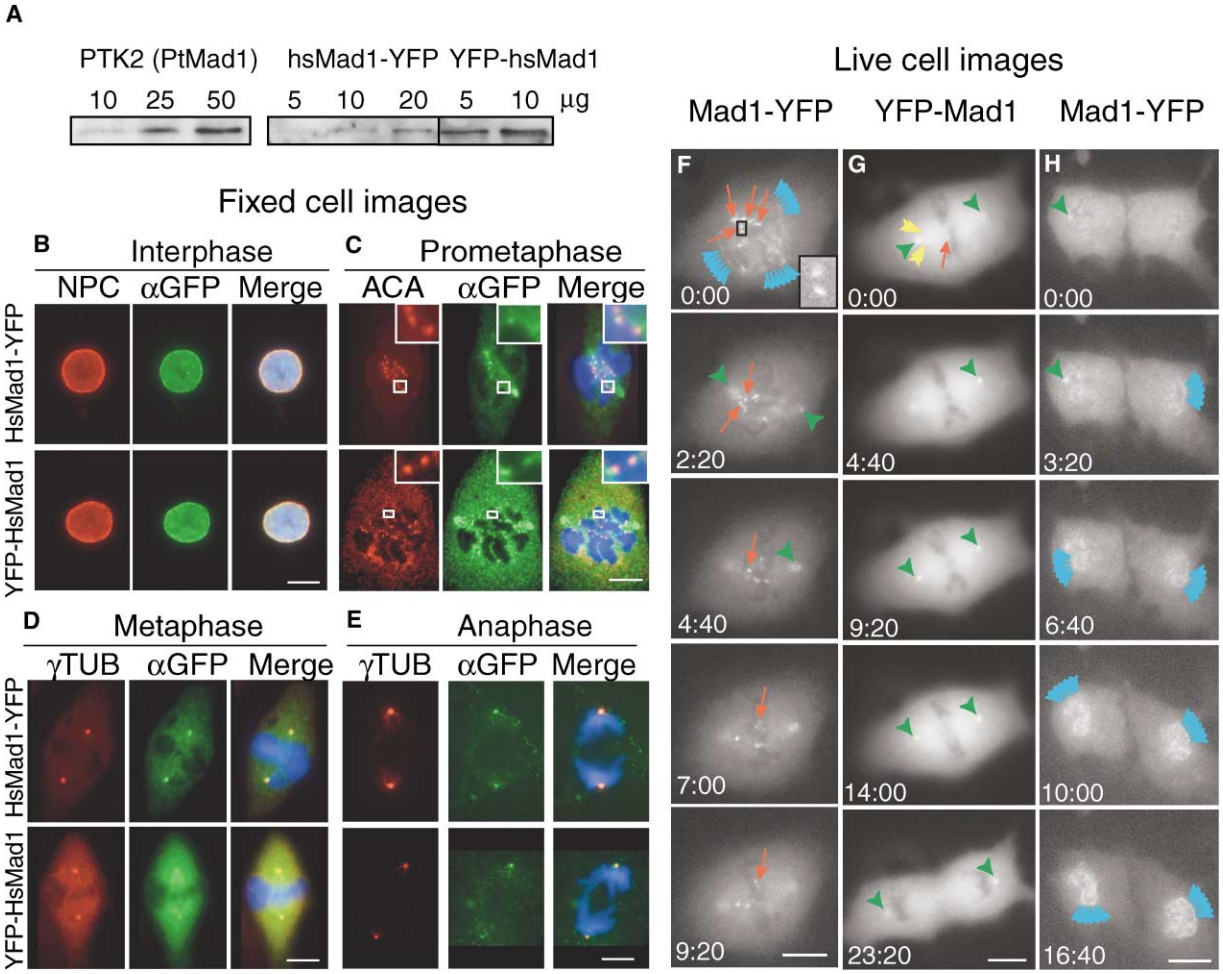

Figure 1. PTK2 Cells Stably Expressing Mad1/YFP

(A) Immunoblots of PTK2 cell lines stably expressing YFP fusions of human Mad1. A dilution series for each cell line was used to estimate the average level of overexpression in the polyclonal cell lines. Fixed-cell immunofluorescence on Mad1/YFP fusions (αGFP, anti-green fluorescent protein) with nuclear-pore complexes (NPC) (B), unattached kinetochores (ACA, anti-centromere antibodies) (C), and spindle poles (γtub, anti-γ-tubulin) in metaphase (D) and anaphase (E) is shown. Also shown are still pictures from live-cell microscopy of PTK2 cells stably expressing HsMad1-YFP (F and H) or YFP-HsMad1 (G) fusion proteins. Specific subcellular structures such as the nuclear envelope (small cyan arrowheads), unattached kinetochores (red arrow), spindle poles (large green arrowheads), and spindle fibers (yellow double arrowheads) become sequentially enriched with Mad1 during mitotic progression. All scale bars represent 10 μm. Time measurements are in minutes and seconds.

increase (approximately 15%) in the length of mitosis (see Figure S1). Immunoblotting with an antibody to hsMad2 (Figure 3A) permitted maximal estimates of approximately 20-fold and 5-fold the level of endogenous PtMad2 for the C-terminal and N-terminal fusions, respectively. Because this antibody almost certainly has lower affinity for PtMad2, it is highly likely that the actual levels were much lower than these estimates, consistent with absence of the kinetochore-independent mitotic arrest previously seen after transient expression of high levels of Mad2 via DNA transfection [19] or in *Xenopus* extracts [21].

The Mad2/YFP fusions localized as previously reported [11] for endogenous PtMad2 and successively accumulated at the nuclear envelope, unattached kinetochores, and spindle poles in fixed-cell immunofluorescence and live-cell imaging (see Figure S1). Although Mad2's binding partner Mad1 was immobilized at kinetochores, both C- and N-terminal fusions of Mad2 partially recovered at kinetochores during normal mitoses (Figure 3C; R% = 60.0% ± 2.7 SEM; $t_{1/2}$ = 10.8 s ± 1.2 SEM, n = 60) or in nocodazole-treated, mitotic checkpoint-arrested cells (Figure 3F; R% = 53.8% ± 3.1 SEM; $t_{1/2}$ = 6.4 s ± 0.7 SEM, n = 59). Mad2 that accumulated near spindle poles after microtubule attachment continued to cycle as rapidly and to a similar recovery percentage as Mad2 at kinetochores (Figures 3C and 3G; R = 55.9% ± 5.0 SEM, $t_{1/2}$ = 7.7 s ± 1.4 SEM, n = 21). Rapid release and rebinding was selective for mitotic Mad2; FRAP of Mad2 bound to the nuclear surface in interphase recovered very slowly (Figures 3B and 3E; R% < 20%, $t_{1/2}$ > 15 min, n = 39 cells), consistent with a stable Mad1-Mad2 complex attached to the nuclear envelope. (Unlike for Mad1 [Figure 3B], the entire nucleoplasmic fluorescence of Mad2 was rapidly reduced after local photobleaching ($t_{1/2}$ < 5 s, n = 39 cells), implicating

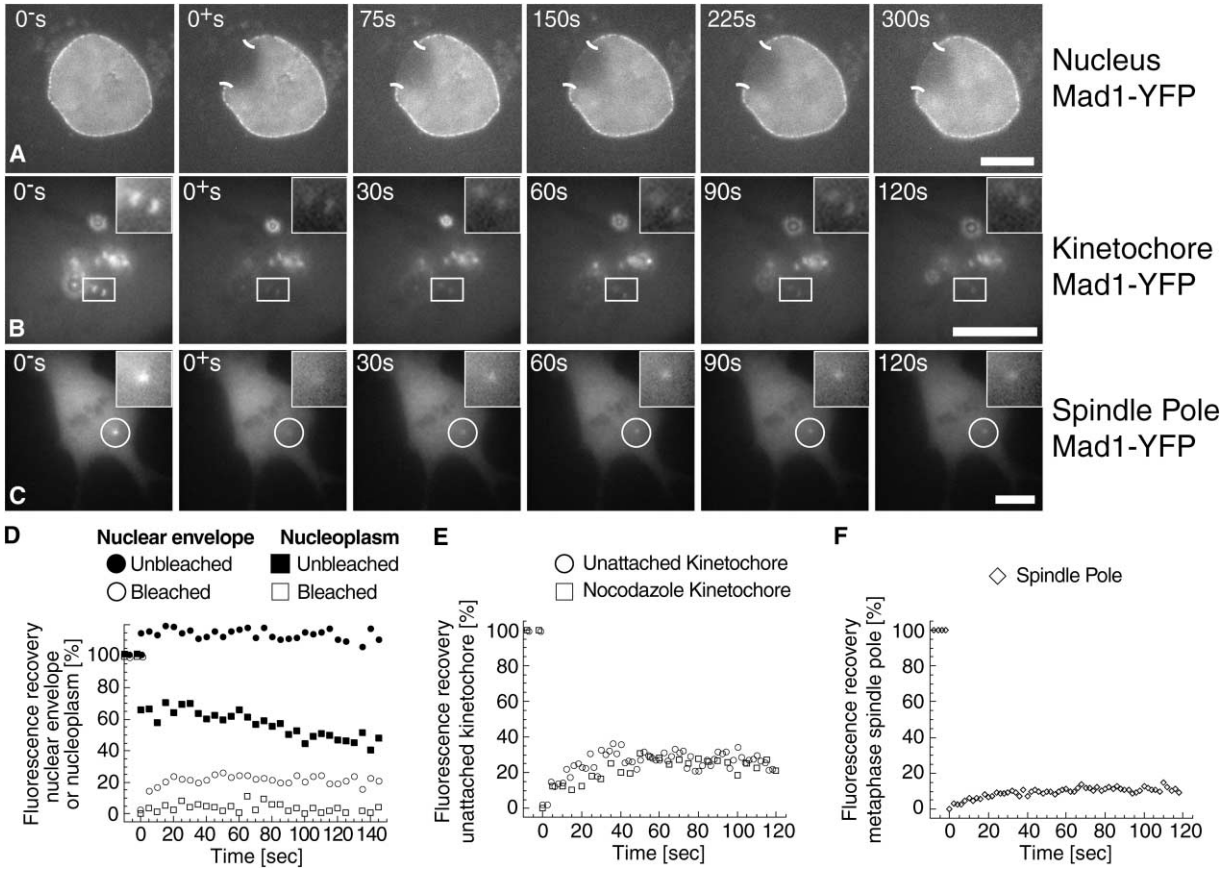

Figure 2. Mad1 Is Stably Bound in the Nucleus, at Unattached Kinetochores, and at Spindle Poles

(A) Time series showing the absence of fluorescence recovery of the nuclear envelope and nucleoplasm over a 5 min period in a Mad1-YFP cell. (B) Time series showing the fluorescence recovery of an unattached kinetochore over a 2 min period in a Mad1-YFP cell (rectangle). (C) Time series showing the fluorescence recovery of a spindle pole late in mitosis over a 2 min period in a Mad1-YFP cell (circle). All scale bars represent 10 μm. Time measurements are in seconds. (D) Fluorescence recovery curve for Mad1/YFP fusion protein at a bleached nuclear envelope (open circles) and in the nucleoplasm (open squares) and an unbleached portion of the same nuclear envelope (filled circles) and nucleoplasm (filled squares). (E) Fluorescence recovery curves for Mad1 YFP-fusion proteins at an unattached kinetochore (open circle) and a nocodazole-blocked kinetochore (open square). (F) Fluorescence recovery curves for Mad1 YFP-fusion proteins at a metaphase spindle pole (open diamond).

a fast diffusive redistribution of the bleached nucleoplasmic pool of Mad2/YFP [Figure 3B].)

To further test the transient component of Mad2, we serially photobleached unattached kinetochores (see Figure 4). The first photobleaching event resulted in approximately 50% recovery (R% = 53.3 ± 1.8 SEM, n = 10), whereas the second resulted in almost complete recovery (R% = 86.8 ± 2.6 SEM, n = 10) (see Figure 4D). The increased efficiency of recovery after the second photobleaching event was also seen with nocodazole-blocked cells (R_1% = 48.9 ± 2.0 SEM to R_2% = 82.8 ± 4.5 SEM n = 11, see Figure 4D). The increase in the subsequent bleaching event demonstrates that the initial pool of recovered Mad2 is indeed transiently associated with unattached kinetochores. In addition, the increased recovery (approximately 90%) indicates that the system is capable of measuring essentially complete recovery of photobleached fluorophores.

Mad1 Is Saturated with Mad2 in Interphase and Early in Mitosis

The stability of Mad2 binding at the nuclear envelope in interphase versus its rapid release and rebinding during mitosis may reflect a cell cycle-dependent change in Mad1-Mad2 affinity. To test this, we generated HeLa cells that stably express YFP fusions of Mad1 or Mad2. Endogenous Mad1 concentration was determined to be approximately 20 nM by quantitative immunoblotting, with purified recombinant Mad1 used as a standard (Figure 5A). This is 10 times lower than Mad2 measured in a similar manner in the same lysates (approximately 200 nM, Figure 5B). The cells stably expressing the YFP-Mad1 fusion accumulated it to approximately five times (or about 100 nM) the endogenous level (Figure 5C) (similar to results for the PTK2 stable line; data not shown).

YFP fusions of Mad1 or Mad2 were depleted from cell lysates by immunoprecipitation (Figure 5C, unbound lanes) and coprecipitated proteins were detected by immunoblotting. In Mad1/YFP cells, anti-GFP depletions coprecipitated little, if any, of the endogenous HeLa Mad1 (Figure 5C, lane 3), demonstrating that even when highly expressed, the YFP fusions do not form dimers or higher oligomers with the endogenous Mad1, in contrast with what has been proposed for Mad1 in some models of the mitotic checkpoint [18, 22]. In both randomly cycling and mitotic cells, Mad1/YFP fusion immunoprecip-

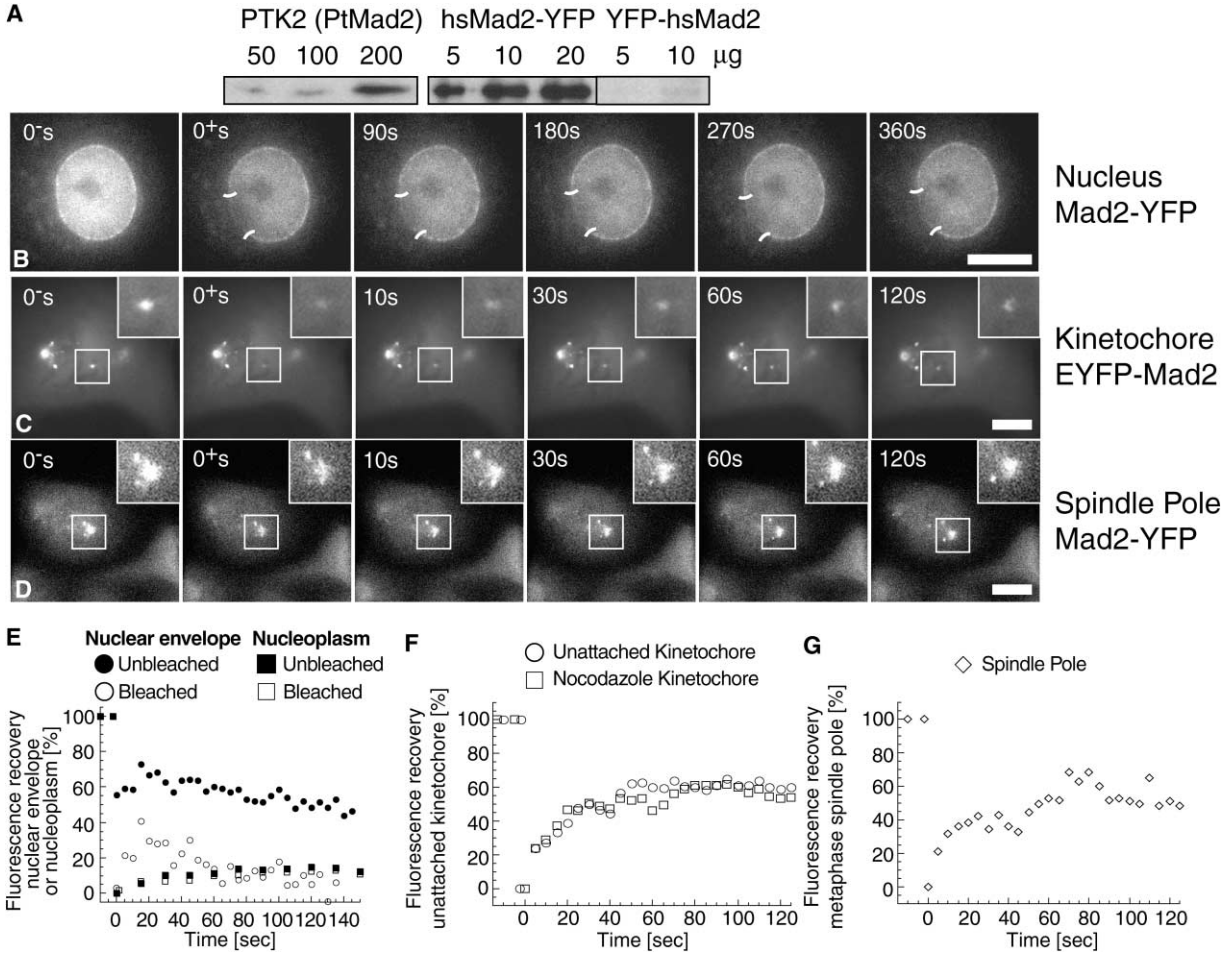

Figure 3. A Portion of Mitotic Mad2 Is Stably Associated with Unattached Kinetochores and Spindle Poles

(A) Immunoblots of PTK2 cell lines stably expressing YFP fusions of human Mad2. A dilution series for each cell line was used for estimating the average level of overexpression in the polyclonal cell lines. (B) Time series showing the absence of fluorescence recovery of the nuclear envelope and fast fluorescence recovery in the nucleoplasm over a 6 min period in a Mad2-YFP cell. (C) Time series showing the partial fluorescence recovery of an unattached kinetochore over a 2 min period in a YFP-Mad2 cell (square). (D) Time series showing the partial fluorescence recovery of a spindle pole late in mitosis over a 2 min period in a Mad2-YFP cell (square). All scale bars represent 10 μm. Time measurements are in seconds. (E) Fluorescence recovery curve for Mad2/YFP fusion protein at a bleached nuclear envelope (open circles) and in the nucleoplasm (open squares) and an unbleached portion of the same nuclear envelope (filled circles) and nucleoplasm (filled squares). (F) Fluorescence recovery curves for a Mad2 YFP-fusion protein at an unattached kinetochore (open circle) and a nocodazole-blocked kinetochore (open square). (G) Fluorescence recovery curves for Mad2 YFP-fusion protein at spindle poles (open diamond).

itates also contained a significant proportion (approximately 50%) of the total Mad2 independently of the position of the YFP (data not shown), whereas Mad2/YFP immunoprecipitation codepleted all endogenous Mad1 (Figure 5C, lanes 2 and 7). Mad2/YFP fusions also coprecipitated endogenous Mad2 both in randomly cycling and in mitotic cells (Figure 5C, lanes 3 and 8), indicating the presence of complexes with two or more molecules of Mad2, as previously postulated [12, 19, 22].

The data above demonstrate that Mad1 is saturated with Mad2 in randomly cycling cells and early in mitosis (nocodazole). However, immunofluorescence and live imaging have demonstrated that although Mad2 dissociates from the pole at anaphase, Mad1 stays bound to spindle poles until late telophase. Thus, most spindle bound Mad1 does not remain bound to Mad2 after anaphase, i.e., after the spindle checkpoint has been satisfied.

CENP-C and Bub1 Are Both Stable Components of Kinetochores

To investigate the possible kinetochore stability of other checkpoint proteins, we expressed YFP fusions of the constitutive centromeric protein, CENP-C, and the kinetochore kinase Bub1, known to be essential for the mitotic checkpoint in yeast [23–25] and metazoans [26–29]. For both fusion proteins, expression by transient transfection resulted in kinetochore localization during mitosis (Figures 5A and 5B). Throughout mitosis, both proteins remained bound to kinetochores, although Bub1 decreased in intensity after kinetochore attachment. Unlike Mad1 and Mad2, Bub1 and CENP-C did not relocalize to spindle poles after kinetochore capture (Figures 6A and 6B).

Upon photobleaching, neither CENP-C nor Bub1 recovered significantly during normal mitosis (Figures 5C and 5D, CENP-C: R% $<$ 10%, $t_{1/2} > 15$ min, n = 20;

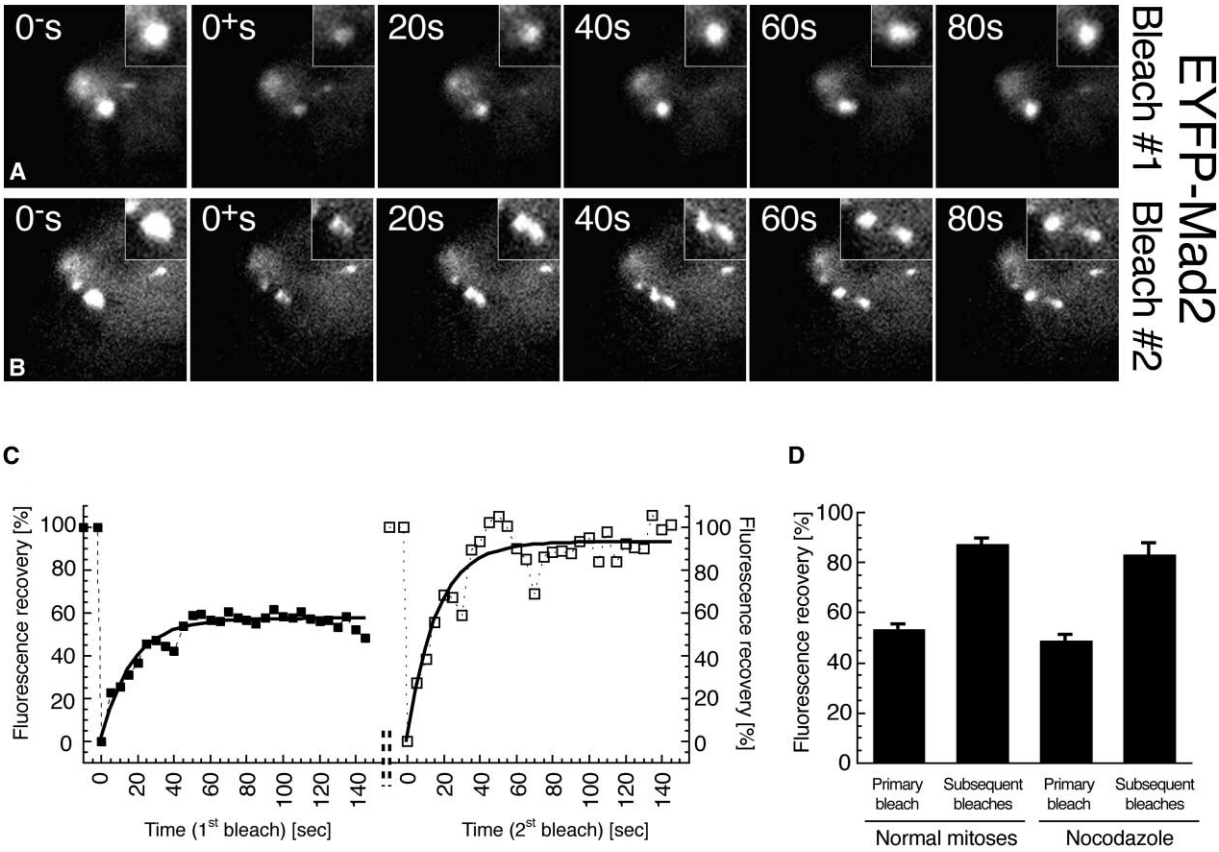

Figure 4. Transient Pool of Mad2 Recovers Completely

(A) Time series of two serial bleaches of an unattached kinetochore. The first bleach eliminates the stable pool and a transient component, whereas the second bleach eliminates only the transient pool. (B) Fluorescence recovery curves for the serial bleachings. (C) Average recovery percentage for first bleach versus subsequent bleaches in normal mitoses and in the presence of nocodazole. All scale bars represent 10 μm. Time measurements are in seconds.

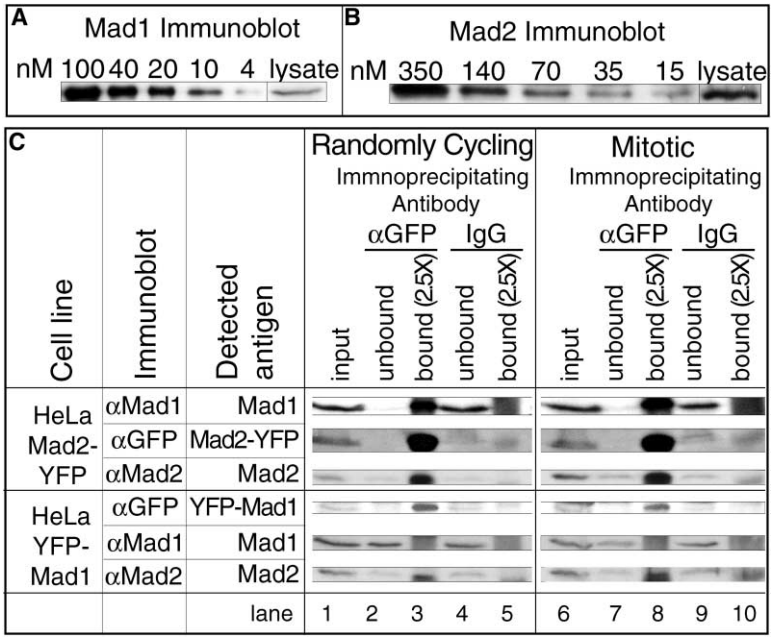

Figure 5. Mad1 Is Saturated with Mad2 throughout the Cell Cycle

(A) A dilution series of recombinant Mad1 protein and HeLa cell lysate shows intracellular Mad1 concentration. (B) A dilution series of recombinant Mad2 protein and HeLa cell lysate shows intracellular Mad2 concentration. (C) HeLa cell lysates stably expressing YFP-Mad1 or Mad2-YFP were immunoprecipitated with anti-GFP antibodies or an IgG control. Immunoblots of input cell lysates (input), unbound supernatant, and IP bound material (2.5× loaded) are shown.

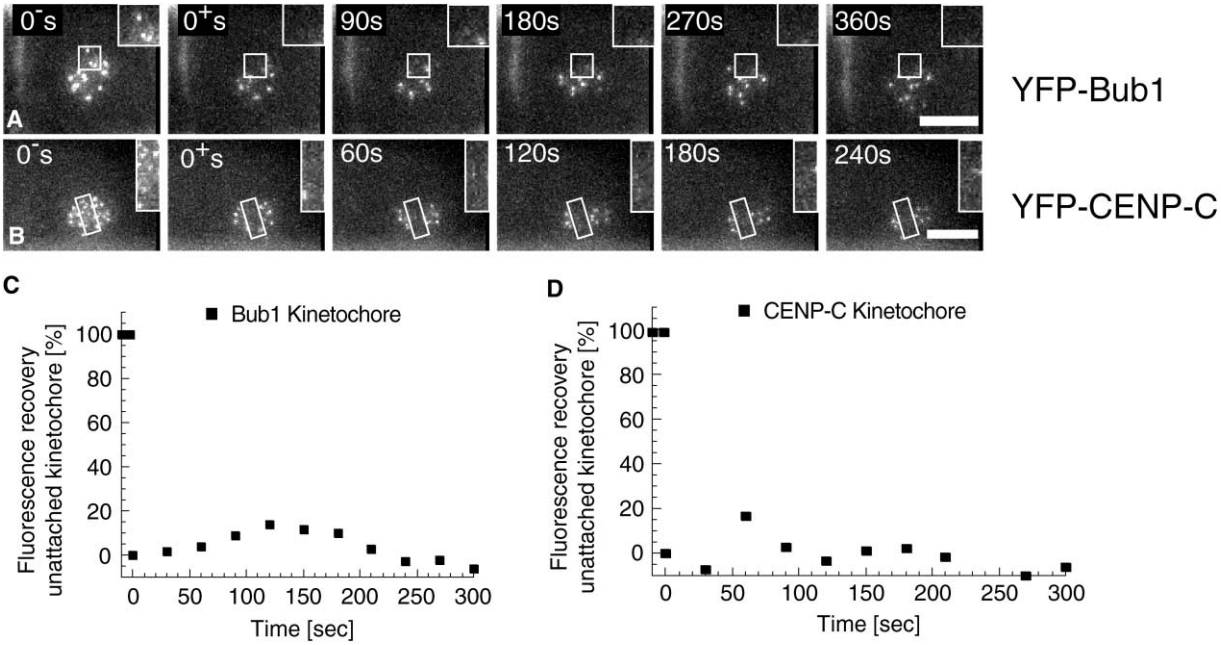

Figure 6. CENP-C and Bub1 Are Stable Components of Kinetochores throughout Early Mitosis

(A) Time series showing the absence of fluorescence recovery of unattached and attached kinetochores over a 6 min period in a YFP-Bub1 cell (rectangle). (B) Time series showing the absence of fluorescence recovery of unattached and attached kinetochores over a 4 min period in a YFP-CENP-C cell (rectangle). All scale bars represent 10 μm. Time measurements are in seconds. (C) Fluorescence recovery curve for YFP-Bub1 fusion protein at a kinetochore (closed square). (D) Fluorescence recovery curve for YFP-CENP-C fusion protein at a kinetochore (closed square).

Bub1: R% $<$ 10%, $t_{1/2} > 15$ min, n = 21) or when the mitotic checkpoint was maximally signaling after nocodazole treatment (Figures 6C and 6D).

Discussion

A Role for an Immobile Mad1/Mad2 Complex at the Nuclear Envelope?

Mad1 and Mad2 are immobilized together at the nuclear envelope (Figure 7A), similar to the static binding known for other envelope components, including nuclear pore complexes [30]. A role for mitotic checkpoint proteins (including Mad1 and Mad2) at the nuclear pore has been proposed in yeast [31], specifically in nuclear transport. In addition, the Bub3 paralog (or analog) Rae1 has been implicated in nuclear transport [32]. Altogether, the data firmly suggest an as-yet-unidentified interphase role for mitotic checkpoint proteins at nuclear pores. The relocalization of Mad1 and Mad2 to unattached kinetochores at mitotic onset has also been seen for *bona fide* nuclear pore complex components [33], indicating a possible pre-kinetochore complex that may exist at the nuclear envelope in interphase.

Stably Bound and Rapidly Cycling Mad2 at Kinetochores

We have shown here that Mad1 is saturated with Mad2 during much of the cell cycle. Despite this, the stable association of Mad2 at the nuclear envelope abruptly changes after nuclear envelope disassembly and attachment of the Mad1-Mad2 complex to unattached kinetochores; Mad1 is stably bound, whereas a proportion of the Mad2 rapidly releases and rebinds. Thus, Mad1 initially recruits Mad2 to these kinetochores, but Mad2 is rapidly released and a new Mad2 subunit recruited from the large cytoplasmic pool. Previous work after microinjection of fluorescently tagged Mad2 in early mitosis or in cells transiently expressing GFP-tagged Mad2 had reported a full recovery (R% = 100) after photobleaching of Mad2 at unattached kinetochores [11]. Here, using stable expression of modest levels of Mad2, we have shown that the recovery of Mad2 is significantly lower (R% $\approx$ 55%). This discrepancy is not due to a limited pool of YFP/Mad2 fusions available for recovery in the stably transfected cells because serial photobleaching of kinetochores results in approximately 90% recovery. Moreover, serial photobleaching demonstrates that the initial kinetochore bound pool of Mad2 is comprised of approximately equal amounts of rapidly exchangeable Mad2 and an equivalent proportion that does not turnover within the few minutes between serial photobleaches. This stable pool is seen in our cell lines that have expressed steady levels of YFP/Mad2 fusions for more than 20 generations but was not observed after microinjection of fluorescently tagged Mad2 early in mitosis or transient expression of what may be very high levels of Mad2 [11]. The simplest resolution of these contrasting findings is that the stably bound pool of Mad2 represents the initial Mad2 that was trafficked in late prophase from the nuclear envelope to the kinetochore in association with Mad1 and which associated with Mad1 much earlier in the previous cell cycle. Transiently labeled products,

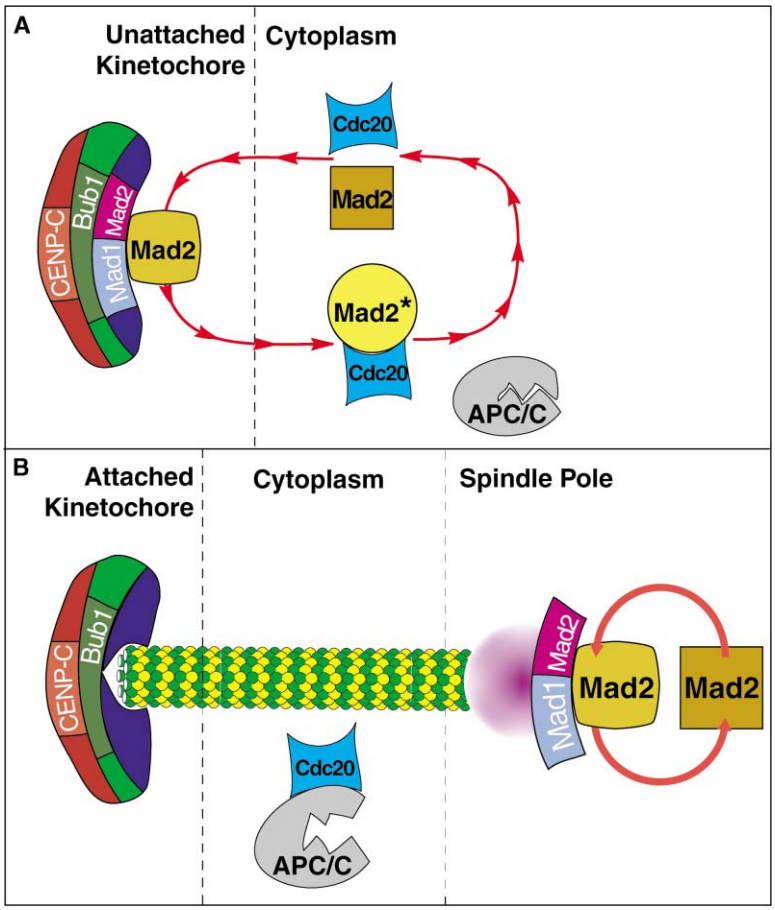

Figure 7. A Model for Checkpoint Activation and Silencing Based on Kinetochore Protein Dynamics

(A) Stable kinetochore components, CENP-C, Bub1, Mad1, and a portion of cellular Mad2 act to activate cytoplasmic Mad2 and produce a "wait-anaphase" signal inhibiting the activity of the APC/C. (B) Upon microtubule attachment, Mad1 and Mad2 relocalize to spindle poles, where a portion of Mad2 remains dynamic but, without the catalytic machinery (e.g., Bub1 remaining at the kinetochore), the Mad2 does not form the "wait signal" and the APC/C is free to ubiquitinate anaphase-promoting substrates.

including those injected after mitotic entry or even synthesized throughout much of the preceding interphase, would not enter this stable pool until subsequent cell cycles.

The Mad1/Mad2 Complex as Part of a Catalytic Platform for Producing a Mad2-Containing "Wait-Anaphase" Signal

Current models of wait-signal generation in the mitotic checkpoint all hinge on the ability of an unattached kinetochore to rapidly produce an at least partially diffusible inhibitor [13]. Because this is facilitated by unattached kinetochores to which a series of essential checkpoint components, including three kinases, must be bound, these kinetochores almost certainly catalyze inhibitor generation and release. From a combination of the stable association of Mad1, a portion of Mad2, Bub1, and CENP-C at unattached kinetochores and the Mad1 requirement for Mad2 recruitment to kinetochores [21, 34], we conclude that Mad1, or more precisely the stable Mad1/Mad2 complex initially recruited to kinetochores, must represent a critical component of the catalytic platform required to prevent anaphase onset.

Fang et al. have previously proposed an oligomerization-based model of Mad2 activation based solely on the products of bacterial expression [12]. The existence of a stable Mad2 population at unattached kinetochores not only provides initial in vivo evidence for multiple Mad2 molecules acting at kinetochores as a component of the signal production cascade but also demonstrates that recruitment of rapidly cycling Mad2 to those kinetochores is through a [Mad1-Mad2]-Mad2 association rather than simply [Mad1]-Mad2 (Figure 7A). Moreover, although a Mad2 mutant (R133A) that is apparently defective in oligomerization binds to unattached kinetochores and produces a robust mitotic arrest [19], the absence of homo-oligomerization of this Mad2 mutant offers no evidence against a continued interaction of the mutant with immobilized, wild-type Mad2 at kinetochores. Indeed, in light of our evidence, this explanation seems likely to us to be how such a Mad2 mutant participates in mitotic arrest.

All of this combines to support a proposal that the Mad1-Mad2 complex forms a core, or scaffold, onto which additional Mad2 molecules may bind [22]. The basis for such a stably bound Mad1-Mad2 complex may lie in a striking Mad2 conformational change upon its binding to Mad1, as suggested by the use of peptides to mimic interactions of the full-length subunits. This has lead to a "safety belt" mechanism in which this conformational change of Mad2 reorients the protein's C terminus to form a loop enclosing its binding region for Mad1 [22, 34]. This leads to the proposal that the immobilized, or scaffolded, Mad1-Mad2 bound at kinetochores is the complex that acts as a template for the catalytic conversion and release of soluble Mad2 mole-

cules in a form that inhibits either Cdc20 or a Cdc20-APC/C complex. The nature of the "activated" Mad2 released from kinetochores remains to be identified.

Silencing Checkpoint Signaling by Dissociation of the Catalytic Mad1/Mad2 Complex after Microtubule Attachment to Kinetochores

Silencing of production of the mitotic checkpoint inhibitor after microtubule capture, for example when CENP-E-mediated binding of spindle microtubules inactivates the essential BubR1 kinase activity at kinetochores [8, 9], forces dissociation of the stably bound Mad1-Mad2 complexes from kinetochores and their relocalization to spindle poles. They are stably bound there and continue rapid cycling of free Mad2 (the recovery percentage for Mad2 after bleaching at poles was similar to that of unattached kinetochores [approximately 56%]). However, without all of the components required for assembly of the catalytic "pocket," this produces only soluble Mad2 or a Mad2 form that is quickly deactivated, rather than an active anaphase inhibitor. Thus, a central aspect of silencing checkpoint signaling is the physical separation of essential components of the catalytic platform (Figure 7B). This hypothesis also predicts that release of the entire catalytic platform (including Mad1 and Mad2) from kinetochores by disruption of Hec1/Ndc80 [35] and could explain why the resulting constitutive checkpoint signaling, presumably via assembly of the entire signaling complex at cytoplasmic sites, cannot be silenced by microtubule attachment at kinetochores. This model is also consistent with the finding that the inability to dissociate kinetochore bound Mad1 from the catalytic machinery, as may occur by the disruption of dynein [36], maintains an assembled catalytic scaffold and therefore prolongs the generation of the Mad2-dependent wait signal (designated Mad2* in Figure 7A) and metaphase arrest, even in the presence of attached kinetochores.

Conclusions

To test central aspects of models governing the mitotic checkpoint, we have visualized and measured the dynamics of CENP-C, Bub1, Mad1, and Mad2. At unattached kinetochores, CENP-C, Bub1, Mad1, and a portion of Mad2 remained stably bound, thereby identifying essential components of a catalytic scaffold responsible for generation of the wait-anaphase signal. Furthermore, the presence of a stable Mad2 pool both at the nuclear envelope and the unattached kinetochore is consistent with recruitment to a stable Mad1/Mad2 complex of additional soluble Mad2 molecules, now in the context of a mitotic kinetochore. Such molecules nclude immobilized Bub1 and collectively result in generation of an activated Mad2 species as a part of the wait-anaphase signal. After attachment, Mad1 and Mad2 are relocalized to the spindle pole, whereas Bub1 remains at kinetochores, providing a mechanism by which to separate the recruiting and catalytic elements of the wait-signal generator and thus silencing the mitotic checkpoint.

Experimental Procedures

cDNAs and Generation of YFP Fusions

The full-length human Mad1 cDNA was kindly provided by Robert Hagan and Peter Sorger (Massachusetts Institute of Technology, Cambridge, MA) and the full-length human Mad2 cDNA from Gouwei Fang (Stanford University, Stanford, CA). Full-length human Bub1 and CENP-C cDNAs were kindly provided by Frank McKeon (Harvard Medical School, Boston, MA).

Human Mad1 was fused to YFP through the insertion of a 3′ Hind III site by polymerase chain reaction (PCR). Sequencing the modified Mad1 confirmed the absence of PCR-induced errors. A BamHI/HindIII Mad1 fragment was ligated into a BglII/HindIII-digested EYFP-C1 (BD Biosciences Clontech, Palo Alto, CA) and a BglII/HindIII-digested version of EYFP-N1 (BD Biosciences Clontech, Palo Alto, CA) that lacked the initial start codon of EYFP. 5′ KpnI and 3′ BamHI sites were used for fusing human Mad2 to the N- and C termini of EYFP in a similar fashion at Mad1. The fusion cDNAs for Mad1 and Mad2 were then excised from each vector through an AfeI/MfeI digestion and ligated into the SnaBI/EcoRI site of the pBABEblast vector, a version of pBABEpuro [38] with a blasticidin resistance marker.

YFP-Bub1 and YFP-CENP-C were generated by excision of the cDNAs from the provided vectors without any PCR-based modifications and inserted into EYFP-C1 and EYFP-C3, respectively (BD Biosciences Clontech, Palo Alto, CA).

Cell Culture

PTK2 (Male potoroo *Potorous tridactylus* kidney epithelial cells) and all derived cell lines were cultured in minimal essential media supplemented with Earle's Salts (MEM-Earle's, Invitrogen, Carlsbad, CA), 10% fetal bovine serum, 0.11 mg/ml sodium pyruvate, 1% nonesential amino acids, 100 U/ml penicillin, and 100 μg/ml streptomycin. All cell culture reagents were purchased from Invitrogen (Carlsbad, CA) unless otherwise specified. All chemicals were purchased from Sigma-Aldrich (St. Louis, MO) unless otherwise specified.

For live-cell analysis, cells were cultured in glass-bottomed chambers (Warner Instruments, Hamden, CT) and the media were replaced with Leibovitz's (L-15)-based media (supplemented with 5% fetal bovine serum, 2.5 mM HEPES [pH 7.2], 4.5 mg/ml glucose, 0.11 mg/ml sodium pyruvate, nonessential amino acids, 100 U/ml penicillin, and 100 μg/ml streptomycin) before being viewed.

293-GP cells, which harbor *gag* and *pol* genes from the Moloney murine leukemia retroviral genome, HeLa cells, and derived cells were cultured in Dulbecco's MEM supplemented with 10% fetal bovine serum, 0.3 mg/ml glutamine, 100 U/ml penicillin, and 100 μg/ml streptomycin.

Generation and Characterization of Stable Cell Lines

Retroviral plasmids (pBABEblast-YFP fusions) were cotransfected into 293-GP cells along with the VSV-G pseudotyping plasmid for the production of amphotropic retrovirus [37] (Fugene, Roche Applied Science, Indianapolis, IN). The resulting retroviral supernatant was mixed with 8 μg/ml hexadimethrine bromide (Polybrene, Sigma-Aldrich, St. Louis, MO) and incubated with PTK2 or HeLa cells for 12 hr. Media were replaced, and the cells were split for selection in 2 μg/ml blasticidin after 48 hr. After two weeks of selection, cells were subjected to flow cytometry (FACSVantage, BD Biosciences, San Jose, CA) for selection of the brightest population (top 5%) and maintained as a polyclonal line.

Transient transfection of YFP fusion cDNAs was accomplished through the use of the Fugene (Roche Applied Science, Indianapolis, IN) according to the manufacturer's recommended protocol.

Analysis of Stable-Line Protein Expression and Immunoprecipitations

To check protein overexpression in stable lines, we trypsinized cells from an 80% confluent 100 mm dish and washed them twice in PBS before lysing them in a modified RIPA buffer (10 mM Phosphate buffer [pH 7.2], 150 mM NaCl, 10 mM EDTA, 1% NP-40, 1% TX-100, and 0.1% SDS) for 10 min on ice. Mitotic arrest was induced by the addition of nocodazole (Sigma-Aldrich, St. Louis, MO) to 330 nM. Protein concentrations were carried out on the soluble supernatant from lysed cells (10,000 × g, 10 min at 4°C) via the BCA method (Pierce Chemical Co., Rockford, IL). SDS-PAGE analysis was carried out on cell lysate samples of equal protein content [38]. Immunoblotting was carried out according to standard protocols [39]. For immunoprecipitations from polyclonal HeLa lines, soluble lysates were

incubated with 10 μg anti-GFP or rabbit IgG antibodies and IgG-antigen complexes collected with Protein A magnetic particles (Dynal Corporation, Lake Success, NY) and washed extensively. Immunoprecipitations were analyzed by SDS-PAGE and immunoblotting via standard methods. Polyclonal rabbit anti-Mad1 antibodies were kindly provided by Michael Campbell and Tim Yen (Fox Chase Cancer Center, Philadelphia, PA) [20] and Kuan-Teh Jeang (Johns Hopkins University, Baltimore, MD) [40]. Monoclonal Mad2 antibodies were obtained commercially (BD Biosciences, San Diego, CA).

Fixed-Cell Indirect Immunofluorescence

Indirect immunofluorescence was carried out via cold-methanol (−20°C) fixation according to standard methods. Anti-nuclear pore complex antibodies (Mab 1414, Covance Research Products, Berkeley, CA), anti-γ-tubulin antibodies (Sigma, St. Louis MO), and anti-human Mad2 antibodies (BD Biosciences, San Diego, CA) were commercially obtained. Anti-centromere antibodies obtained from human autoimmune serum were a kind gift of Kevin Sullivan (Scripps Research Institute, La Jolla, CA). DNA was stained with DAPI, and fixed-cell preparations were mounted in Vectashield (Vector Laboratories, Burlingame, CA) supplemented with 10 mM $MgCl_2$.

Live-Cell Microscopy and FRAP Instrumentation

Live-cell images were taken on a Nikon Eclipse 300 inverted microscope (Nikon USA, Melville, NY) with a 60× or 100× high-numerical aperture (NA 1.4) Plan Apochromat objective lens. Cells were kept at 35°C by a stage heater that accommodated glass-bottomed 35 mm dishes (Warner Instruments Inc., Hamden, CT). Images were collected with a Photometrics COOLSNAP HQ camera (Roper Scientific, Tuscon, AZ) (gain = 2, 10 MHz) and captured on a computer through the use of the Metamorph software system (Universal Imaging Corp., Downingtown, PA). Time-lapse sequences were captured with exposure times of 300 ms, at 2 × 2 binning and with interframe intervals from 2 to 30 s.

Some fluorescence recovery after photobleaching experiments were carried out on a Zeiss Axiovert 200TV inverted microscope (Carl Zeiss International, Thornwood, NY) equipped with a 63× (high NA 1.4) Plan Apochromat objective lens. Images were collected with a Photometrics Quantix B57 camera (Roper Scientific, Tuscon, AZ). The imaging system was controlled via the Labview software system (National Instruments). Photobleaching was carried out with the 532 nm line of an Nd:YAG (76 MHz, 70 ps pulse width) laser at 20 mW, measured at the backplane of the objective. The laser was focused onto the backplane of the objective through the lower imaging port of the microscope. Other FRAP experiments were conducted with a nitrogen dye (514 nm dye cell) laser system (Photonics Instruments, Chicago, IL) adapted onto the live-cell apparatus described above. All the constructs behaved similarly under both FRAP systems.

Fluorescence Recovery after Photobleaching Analysis

Analysis of recovery after photobleaching was done with the Metamorph software package. Kinetochore and spindle pole recoveries were carried out according to [41] and [11]. In brief, two concentric regions, A_{large} and A_{small}, around the kinetochore or spindle pole were delineated. Integrated intensities in both regions (I_{large} and I_{small}) were measured, and background-subtracted fluorescence was calculated according to $I_{signal} = I_{small} - (I_{large} - I_{small})/(A_{large} - A_{small}) \times A_{small}$. Half recovery times (t1/2) were calculated according to $t_{1/2} = \ln(2)/k$, where k is the time constant for a single exponential recovery model. Recovery percentage was taken as the final plateau intensity minus the postbleach intensity, all divided by the difference between pre- and postbleach intensities. To ensure that no significant photobleaching of the free YFP fusions pool was taking place, we checked the background (integrated intensity between the concentric regions) for each measurement. If significant background photobleaching (<95% original value at the end of the experiment) occurred, that particular recovery measurement was excluded from the analysis. All recovery measurements were well fitted by single exponential recovery kinetics (Kaleidagraph, Synergy Software, Reading, PA). Nuclear envelope and nucleoplasm recovery were measured simultaneoulsy at bleached and nonbleached regions within the same nucleus and then corrected for background bleaching with a cytoplasmic fluorescence measurement.

Acknowledgments

The authors would like to thank Tatiana Kraseiva, Zifu Wang and the National Institutes of Health Laser Microbeam and Medical Program (RR 01192) facility at the Beckman Laser Institute for help with initial FRAP studies and the University of California-San Diego Cancer Center Flow Cytometry facility for technical assistance. We also thank an anonymous referee for the very useful suggestion of repetitive photobleaching as a way of identifying stable and more rapidly exchangeable fractions of kinetochore bound Mad2. E.B. thanks the generous support of the Beckman Fellows program. This work was supported in part by grants from the National Institutes of Health to D.W.C. (GM 29513) and M.B. (RR 14892) and from the Air Force Office of Scientific Research (F49620) to M.B. Additionally, D.W.C. receives salary support from the Ludwig Institute for Cancer Research.

Received: November 25, 2003
Revised: March 11, 2004
Accepted: March 16, 2004
Published: June 8, 2004

References

1. Amon, A. (1999). The spindle checkpoint. Curr. Opin. Genet. Dev. *9*, 69–75.
2. Cleveland, D.W., Mao, Y., and Sullivan, K.F. (2003). Centromeres and kinetochores: from epigenetics to mitotic checkpoint signaling. Cell *112*, 407–421.
3. Millband, D.N., Campbell, L., and Hardwick, K.G. (2002). The awesome power of multiple model systems: interpreting the complex nature of spindle checkpoint signaling. Trends Cell Biol. *12*, 205–209.
4. Hoyt, M.A. (2001). A new view of the spindle checkpoint. J. Cell Biol. *154*, 909–911.
5. Peters, J.M. (2002). The anaphase-promoting complex: proteolysis in mitosis and beyond. Mol. Cell *9*, 931–943.
6. Rieder, C.L., Cole, R.W., Khodjakov, A., and Sluder, G. (1995). The checkpoint delaying anaphase in response to chromosome monoorientation is mediated by an inhibitory signal produced by unattached kinetochores. J. Cell Biol. *130*, 941–948.
7. Nicklas, R.B., Ward, S.C., and Gorbsky, G.J. (1995). Kinetochore chemistry is sensitive to tension and may link mitotic forces to a cell cycle checkpoint. J. Cell Biol. *130*, 929–939.
8. Mao, Y., Abrieu, A., and Cleveland, D.W. (2003). Activating and silencing the mitotic checkpoint through CENP-E-dependent activation/inactivation of BubR1. Cell *114*, 87–98.
9. Weaver, B.A.A., Bonday, Z.Q., Putkey, F.R., Kops, G.J.P.L., Silk, A.D., and Cleveland, D.W. (2003). CENP-E is essential for the mammalian mitotic checkpoint to prevent aneuploidy due to single chromosome loss. J. Cell Biol. *162*, 551–563.
10. Dobles, M., Liberal, V., Scott, M.L., Benezra, R., and Sorger, P.K. (2000). Chromosome missegregation and apoptosis in mice lacking the mitotic checkpoint protein Mad2. Cell *101*, 635–645.
11. Howell, B.J., Hoffman, D.B., Fang, G., Murray, A.W., and Salmon, E.D. (2000). Visualization of Mad2 dynamics at kinetochores, along spindle fibers, and at spindle poles in living cells. J. Cell Biol. *150*, 1233–1250.
12. Fang, G., Yu, H., and Kirschner, M.W. (1998). The checkpoint protein MAD2 and the mitotic regulator CDC20 form a ternary complex with the anaphase-promoting complex to control anaphase initiation. Genes Dev. *12*, 1871–1883.
13. Shah, J.V., and Cleveland, D.W. (2000). Waiting for anaphase: Mad2 and the spindle assembly checkpoint. Cell *103*, 997–1000.
14. Kallio, M.J., Beardmore, V.A., Weinstein, J., and Gorbsky, G.J. (2002). Rapid microtubule-independent dynamics of Cdc20 at kinetochores and centrosomes in mammalian cells. J. Cell Biol. 158, 841–847. Published online August 26, 2002. DOI: 10.1083/jcb.200201135.
15. Hori, T., Haraguchi, T., Hiraoka, Y., Kimura, H., and Fukagawa, T. (2003). Dynamic behavior of Nuf2-Hec1 complex that localizes to the centrosome and centromere and is essential for

mitotic progression in vertebrate cells. J. Cell Sci. *116*, 3347–3362.
16. McCleland, M.L., Gardner, R.D., Kallio, M.J., Daum, J.R., Gorbsky, G.J., Burke, D.J., and Stukenberg, P.T. (2003). The highly conserved Ndc80 complex is required for kinetochore assembly, chromosome congression, and spindle checkpoint activity. Genes Dev. *17*, 101–114.
17. Musacchio, A., and Hardwick, K.G. (2002). The spindle checkpoint: structural insights into dynamic signalling. Nat. Rev. Mol. Cell Biol. *3*, 731–741.
18. Yu, H. (2002). Regulation of APC-Cdc20 by the spindle checkpoint. Curr. Opin. Cell Biol. *14*, 706–714.
19. Sironi, L., Melixetian, M., Faretta, M., Prosperini, E., Helin, K., and Musacchio, A. (2001). Mad2 binding to Mad1 and Cdc20, rather than oligomerization, is required for the spindle checkpoint. EMBO J. *20*, 6371–6382.
20. Campbell, M.S., Chan, G.K., and Yen, T.J. (2001). Mitotic checkpoint proteins HsMAD1 and HsMAD2 are associated with nuclear pore complexes in interphase. J. Cell Sci. *114*, 953–963.
21. Chen, R.H., Shevchenko, A., Mann, M., and Murray, A.W. (1998). Spindle checkpoint protein Xmad1 recruits Xmad2 to unattached kinetochores. J. Cell Biol. *143*, 283–295.
22. Sironi, L., Mapelli, M., Knapp, S., Antoni, A.D., Jeang, K.T., and Musacchio, A. (2002). Crystal structure of the tetrameric Mad1-Mad2 core complex: implications of a 'safety belt' binding mechanism for the spindle checkpoint. EMBO J. *21*, 2496–2506.
23. Meeks-Wagner, D., Wood, J.S., Garvik, B., and Hartwell, L.H. (1986). Isolation of two genes that affect mitotic chromosome transmission in S. cerevisiae. Cell *44*, 53–63.
24. Pangilinan, F., and Spencer, F. (1996). Abnormal kinetochore structure activates the spindle assembly checkpoint in budding yeast. Mol. Biol. Cell *7*, 1195–1208.
25. Hoyt, M.A., Totis, L., and Roberts, B.T. (1991). S. cerevisiae genes required for cell cycle arrest in response to loss of microtubule function. Cell *66*, 507–517.
26. Fukagawa, T., Pendon, C., Morris, J., and Brown, W. (1999). CENP-C is necessary but not sufficient to induce formation of a functional centromere. EMBO J. *18*, 4196–4209.
27. Basu, J., Bousbaa, H., Logarinho, E., Li, Z., Williams, B.C., Lopes, C., Sunkel, C.E., and Goldberg, M.L. (1999). Mutations in the essential spindle checkpoint gene bub1 cause chromosome missegregation and fail to block apoptosis in Drosophila. J. Cell Biol. *146*, 13–28.
28. Sharp-Baker, H., and Chen, R.H. (2001). Spindle checkpoint protein Bub1 is required for kinetochore localization of Mad1, Mad2, Bub3, and CENP-E, independently of its kinase activity. J. Cell Biol. *153*, 1239–1250.
29. Taylor, S.S., and McKeon, F. (1997). Kinetochore localization of murine Bub1 is required for normal mitotic timing and checkpoint response to spindle damage. Cell *89*, 727–735.
30. Daigle, N., Beaudouin, J., Hartnell, L., Imreh, G., Hallberg, E., Lippincott-Schwartz, J., and Ellenberg, J. (2001). Nuclear pore complexes form immobile networks and have a very low turnover in live mammalian cells. J. Cell Biol. *154*, 71–84.
31. Iouk, T., Kerscher, O., Scott, R.J., Basrai, M.A., and Wozniak, R.W. (2002). The yeast nuclear pore complex functionally interacts with components of the spindle assembly checkpoint. J. Cell Biol. *159*, 807–819.
32. Babu, J.R., Jeganathan, K.B., Baker, D.J., Wu, X., Kang-Decker, N., and van Deursen, J.M. (2003). Rae1 is an essential mitotic checkpoint regulator that cooperates with Bub3 to prevent chromosome missegregation. J. Cell Biol. *160*, 341–353.
33. Belgareh, N., Rabut, G., Bai, S.W., van Overbeek, M., Beaudouin, J., Daigle, N., Zatsepina, O.V., Pasteau, F., Labas, V., Fromont-Racine, M., et al. (2001). An evolutionarily conserved NPC subcomplex, which redistributes in part to kinetochores in mammalian cells. J. Cell Biol. *154*, 1147–1160.
34. Luo, X., Tang, Z., Rizo, J., and Yu, H. (2002). The Mad2 spindle checkpoint protein undergoes similar major conformational changes upon binding to either Mad1 or Cdc20. Mol. Cell *9*, 59–71.
35. Martin-Lluesma, S., Stucke, V.M., and Nigg, E.A. (2002). Role of Hec1 in spindle checkpoint signaling and kinetochore recruitment of Mad1/Mad2. Science *297*, 2267–2270.
36. Howell, B.J., McEwen, B.F., Canman, J.C., Hoffman, D.B., Farrar, E.M., Rieder, C.L., and Salmon, E.D. (2001). Cytoplasmic dynein/dynactin drives kinetochore protein transport to the spindle poles and has a role in mitotic spindle checkpoint inactivation. J. Cell Biol. *155*, 1159–1172.
37. Morgenstern, J., and Land, H. (1990). Advanced mammalian gene transfer: high titre retroviral vectors with multiple drug selection markers and a complementary helper-free packaging cell line. Nucleic Acids Res. *18*, 3587–3596.
38. Laemmli, U.K. (1970). Cleavage of structural proteins during the assembly of the head of bacteriophage T4. Nature *227*, 680–685.
39. Towbin, H., Staehelin, T., and Gordon, J. (1979). Electrophoretic transfer of proteins from polyacrylamide gels to nitrocellulose sheets: procedure and some applications. Proc. Natl. Acad. Sci. USA *76*, 4350–4354.
40. Kasai, T., Iwanaga, Y., Iha, H., and Jeang, K.T. (2002). Prevalent loss of mitotic spindle checkpoint in adult T-cell leukemia confers resistance to microtubule inhibitors. J. Biol. Chem. *277*, 5187–5193.
41. Maddox, P.S., Bloom, K.S., and Salmon, E.D. (2000). The polarity and dynamics of microtubule assembly in the budding yeast Saccharomyces cerevisiae. Nat. Cell Biol. *2*, 36–41.

Note Added in Proof

We call your attention to another paper that also addresses the dynamics of spindle checkpoint proteins at kinetochores in this issue (Howell, B.J., Moree, B., Farrar, E.M., Stewart, S., Fang, G., and Salmon, E.D. [2004]. Spindle checkpoint protein dynamics at kinetochores in living cells. Curr. Biol *14*, 953–964.